Study on The Relative *Trans* Influence of -EPh_3 ligands (E = Pb, or Sn) in pentacarbonylmanganese(I) complexes like $Mn(CO)_5PbPh_3$ and $Mn(CO)_5SnPh_3$.

ABSTRACT

The *trans* influence of -EPh_3 ligands (where E = Pb or Sn) was studied in $Mn(CO)_5PbPh_3$ and $Mn(CO)_5SnPh_3$, and an intermediate for the preparation for $Mn(CO)_5PbPh_3$ was made; namely, Ph_3PbCl. IR spectroscopy and X-Ray crystallography were performed to determine the respective bond strengths of the *trans* Mn–C bonds in $Mn(CO)_5PbPh_3$ and $Mn(CO)_5SnPh_3$. And it was determined that there was no statistically significant difference in the respective *trans* Mn–C bonds between the two compounds, suggesting that a difference in the *trans* influence of -$PbPh_3$ relative to -$SnPh_3$ was not present. IR data showed the *trans* CO vibrational frequencies for both the compounds to be 2092 cm^{-1}, suggesting that no difference in the respective bond strengths of the *trans* Mn–C bonds nor one in the *trans* influence of -$PbPh_3$ versus -$SnPh_3$ ligands existed.

INTRODUCTION:

Trans influence of ligands is an important and critical phenomenon for chemists to study because, if the information about the relative *trans* influence of one ligand over another is known, then they can tailor metallic complexes with specific ligands, which can in turn play an important role in the stability, reactivity, or selectivity of those complexes. And consequently, with different tailoring methods for all sorts of chemical compounds, the boundaries of the many applications of this simple phenomenon are naturally infinite. *Trans* influence was defined as the ability of a ligand to weaken the bond strength of an M-X bond *trans* to it.[1] Moreover, it is important because as mentioned above, metallic complexes can be tailored for several purposes; for example, it has been found that *trans* influence plays a crucial role in the catalytic activity of palladium(II) catalysts and even plays a strong role

in the bioactivity of cisplatin, which is pt(II) anticancer drug used to treat small cell lung, ovarian, testicular, and neck tumors.[2, 3] Moreover, one of the important aspects of palladium(II) catalysts is their ability to promote the borylation of sp^3 hybridized C–H bonds.[4]

In addition, the study of *trans* influence and its effects has largely been on metallic complexes from the d-block of the periodic table[5]; and because nuclear waste management is an important sector of chemical research[5], it was found that an f-block element containing octahedral lanthanum(III) compound consisted of a chloride ligand, whose the *trans* influence on a neutral ligand L^3 was explicitly measured.[5] Moreover, it can be inferred that *trans* influence of ligands bound to f-block elements would be difficult to study due to their largely complex angular properties of the involved f-orbitals.[6] Nonetheless, in addition to the lanthanum(III) complex, the *trans* influence in $(py)_3Yb(SPh)_3$ has also been shown[6] – namely, with the Yb–S bond *trans* to the SPh being shorter than the Yb–S bond *trans* to the pyridine ligand.[6]

In addition, considering the applications of catalysts in organic conversions such as those of gold(I) complexes,[7] and the fact that gold(I) complexes are linear systems,[7] they are used as ideal systems for studying the *trans* influence of ligands.[7] Moreover, the catalytic activity of these gold adducts is very heavily influenced by the electronic environment of the gold centers themselves[7]; therefore, chemists and scientists, due to the *trans* influence of fluorine on ligands in these catalysts, catalytic activity can be modulated by the scientists if they fluorinate the ligands on these gold adducts.[7]

In this experiment, the *trans* influence of different $-EPh_3$ ligands in octahedral Mn(I) complexes (where E = Pb or Sn, which are group 14 elements). As aforementioned, the applications that are possible when the *trans* influence of a particular type of ligand is known are infinite. The applications of Ph_3PbCl, since it is an ionophore[8], are vast because it can be used as an electrode.[8] Not just that, but the ligand $-PbPh_3$ also is found to have applications in catalysts.[9] Therefore, knowing whether $-PbPh_3$ has a *trans* influence on ligands *trans* to them could help scientists tailor metallic complexes to serve as better

catalysts and aid in the decision making process of which functional groups to add to those complexes and so on.

The study of the *trans* influence of $SnPh_3$ is important as well because it has been found to be a ligand in an apoptosis-inducing agent, which was determined using in vivo cell cultures.[10] Therefore knowing whether the -$SnPh_3$ has an explicit *trans* influence could, once again, help chemists tailor reactions to better create cancer drugs.

However, this report is concerned with a relative *trans* influence difference between -$PbPh_3$ and -$SnPh_3$ within Mn(I) complexes and if a trend at all is present within these group 14 elements. Theoretically speaking, it could be expected that since Pb is a heavier and bigger atom, that the bond length between Mn–Pb would be naturally larger than Mn–Sn, and therefore it could be concluded that the *trans* Mn–C bond for MnPb compound vs MnSn compound would be shorter; however, there are many other factors that could possibly play a role in the Mn–Pb and Mn–Sn bond lengths being different, and therefore, in order to ascertain whether a *trans* influence between $Mn(CO)_5PbPh_3$ and $Mn(CO)_5SnPh_3$ existed, the compounds were prepared in a laboratory setting, and spectroscopic methods were employed to determine the relative bond strengths of the *trans* Mn–C bonds, from which the *trans* influence trend could be determined. IR spectroscopy was employed to measure the vibrational frequencies of the *trans* CO bonds, which provide insight into the *trans* influence of the -EPh_3 ligands. X-ray crystallography provided the direct *trans* Mn–C bond lengths, which provided the greatest insight into the relative *trans* influence of both the compounds.

EXPERIMENTAL METHODS:

Synthesis of $MnCO_5SnPh_3$. Mercury (15.224g, 75.90 mmol) and sodium metal (0.1499 g, 6.520 mmol) were added, stirred, and allowed to amalgamate under an N_2 (g) atmosphere. Upon addition of

the pieces of sodium to the mercury, smoke was observed. Decacarbonyldimanganese(0) (0.505 g, 1.295 mmol) was dissolved in 25 mL of N_2 (g) sparged THF and this solution was then sparged for approximately 3 min before being added to the amalgam, which was then allowed to stir for 30 min at room temperature. A yellow color was observed upon addition of the Mn_2CO_{10} in N_2 (g) sparged THF. Upon addition of this yellow solution to the amalgam, a deep milky brown color was observed. A constant flow of N_2 (g) was maintained throughout the entirety of the synthesis. Separately, triphenyltin chloride (1.006 g, 2.61 mmol) was added to 20 mL of N_2 (g) sparged THF, and this solution was then sparged with N_2 (g) for approximately an additional 3 min before being added to the reaction mixture. Upon addition of the triphenyltin chloride to brown reaction mixture, a cloudy yellow green color was observed. This mixture was allowed to stir for 20 min and was then diluted with 10 mL THF and then allowed to stir for 5 additional min. This reaction mixture was vacuum filtered using celite, and the filtrate volume was reduced to ½ of its initial volume. Deionized water was added to this reduced volume of the filtrate until a yellow precipitate stopped forming. This filtrate was vacuum filtered, and the yellow crude product was collected. Recrystallization via hot filtration using hexanes was performed on these crystals and the light yellow product was collected via vacuum filtration. Yield: **97 mg (7 %).** m.p. = 152-156 °C. **^{1}H NMR** (499.24 MHz, $CDCl_3$) δ 7.63 (d, $^{3}J_{H\text{-}H}$ = 5.0 Hz; ^{119}Sn satellites, d, $^{3}J_{H\text{-}Sn}$ = 44.9 Hz; 2H, H-ortho), 7.387 (m, 3H, H-para & H-meta). **^{119}Sn{^{1}H} NMR** (186.39 MHz, $CDCl_3$) δ -10.86.

Synthesis of Ph_3PbCl . The synthesis of Ph_3PbCl was performed as it was commercially unavailable and was needed as a reagent in preparation of Mn(CO)5PbPh3. Tetraphenyllead (2.048 g, 3.972 mmol) was added in 50 mL chloroform at 50°C. HCl (g) was generated by adding NaCl (20.004 g, 342.3 mmol) to 10 mL of H_2SO_4 (aq). From this reaction mixture, HCl (g) was generated and consequently bubbled into the tetraphenyllead and chloroform mixture. This new mixture was now allowed to stir. Upon the white precipitate formation, the bubbling of HCl (g) into the lead mixture was stopped. This

reaction mixture was vacuum filtered and organic solvent was removed via rotary evaporation and the crude product was collected. This crude product was dissolved in ~200 mL of boiling ethanol and vacuum filtered to remove any impurities. Then the ethanol was then removed via rotary evaporation, and the product was collected. **Yield: 1.375 g (73 %)**. m.p. = 196-206 °C. **^{1}H NMR** (499.24 MHz, $CDCl_3$) δ 7.74 (d, $^{3}J_{H\text{-}H}$ = 7.0 Hz, ^{207}Pb satellites, d, $^{3}J_{H\text{-}Pb}$ = 110.0 Hz; 2H, H-ortho), 7.56 (t, $^{3}J_{H\text{-}H}$ = 7.5 Hz, ^{207}Pb satellites, d, $^{4}J_{H\text{-}Pb}$ = 38.94 Hz; 2H, H-meta), 7.42 (t, $^{3}J_{H\text{-}H}$ = 7.5 Hz; 1H, H-para). **^{207}Pb{^{1}H} NMR** (104.55 MHz, $CDCl_3$) δ -177.24.

Synthesis of $Mn(CO)_5PbPh_3$. Mercury (14.88 g, 74.18 mmol) and sodium metal (0.150 g, 6.520 mmol) were added, stirred, and allowed to amalgamate under an N_2 (g) atmosphere. Upon addition of the pieces of sodium to the mercury, smoke was observed. Decacarbonyldimanganese(0) (0.403 g, 1.033 mmol) was dissolved in 25 mL of N_2 (g) sparged THF and this solution was then sparged for approximately 3 min before being added to the amalgam, which was then allowed to stir for 30 min at room temperature. A yellow color was observed upon addition of the Mn_2CO_{10} in N_2 (g) sparged THF. Upon addition of this yellow solution to the amalgam, a deep milky brown color was observed. A constant flow of N_2 (g) was maintained throughout the entirety of the synthesis. Separately, triphenyllead chloride (0.994 g, 2.097 mmol) was added to 20 mL of N_2 (g) sparged THF, and this solution was then sparged with N_2 (g) for approximately an additional 3 min before being added to the reaction mixture. Upon addition of the triphenyllead chloride to the brown reaction mixture, a cloudy yellow green color was observed. This mixture was allowed to stir for 20 min and was then diluted with 10 mL THF and then allowed to stir for 5 additional min. This reaction mixture was vacuum filtered using celite, and the filtrate volume was reduced to ½ of its initial volume. Deionized water was added to this reduced volume of the filtrate until a yellow precipitate stopped forming. Upon addition of DI water, the solution was observed to be of a yellow-orange color. This filtrate was vacuum filtered, and the yellow

crude product was collected. Recrystallization via hot filtration using hexanes was performed on these crystals and the white-yellow product was collected via vacuum filtration. **Yield: 0.133 g (10 %).** m.p. = 240-244°C. **^{1}H NMR** (499.24 MHz, $CDCl_3$) δ 7.63 (d, $^{3}J_{H-H}$ = 7.0 Hz, ^{207}Pb satellites, d, $^{3}J_{H-Pb}$ = 80.9 Hz; 2H, H-ortho), 7.42 (t, $^{3}J_{H-H}$ = 7.0 Hz; 2H, H-meta), 7.35 (t, $^{3}J_{H-H}$ = 7.0 Hz, 1H, H-para). **^{207}Pb{^{1}H} NMR** (104.55 MHz, $CDCl_3$) δ -177.13.

RESULTS:

Characterization of the triphenyllead chloride. Once Ph_3PbCl was synthesized, an NMR sample was prepared for ^{1}H and ^{207}Pb NMR. The appropriate ^{1}H and ^{207}Pb NMR spectra are depicted in the appendix of this report. For infrared spectroscopy, a KBr and Ph_3PbCl pellet was created and the respective IR spectrum is shown below in figure 1, in which, in table 1, the relevant aromatic peaks are labeled.

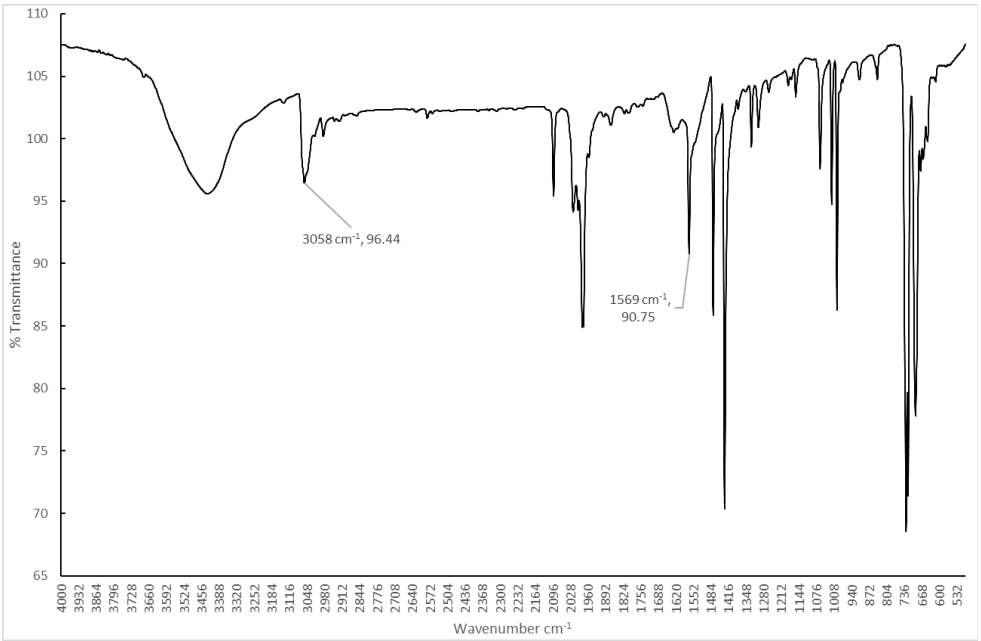

Figure 1. IR Spectrum of KBr-Ph_3PbCl pellet.

Characterization of the $Mn(CO)_5EPh_3$. Once the $Mn(CO)_5EPh_3$ (where E = Pb or Sn) was synthesized, an NMR sample was prepared for ^{1}H , ^{207}Pb, and ^{119}Sn NMR, with the appropriate spectra in

the appendix. For infrared spectroscopy, a KBr and $Mn(CO)_5EPh_3$ pellet was created and the respective IR spectra are shown below in figure 2 and 4 below. In tables 2 and 6, the relevant peak assignments are provided. Structural characterization of $Mn(CO)_5EPh_3$ using X-Ray crystallography was performed, and in figures 3 and 5, the single asymmetric unit of a crystal of $Mn(CO)_5EPh_3$ is depicted. Following the depiction of the single repeating array of $Mn(CO)_5EPh_3$, in tables 3, 4, 5, 7, 8 and 9 below, the appropriate bond lengths (in Å) of the *cis* and *trans* Mn–C bonds, the *cis*-C–O bond lengths and the *trans*-C–O bond lengths are provided.

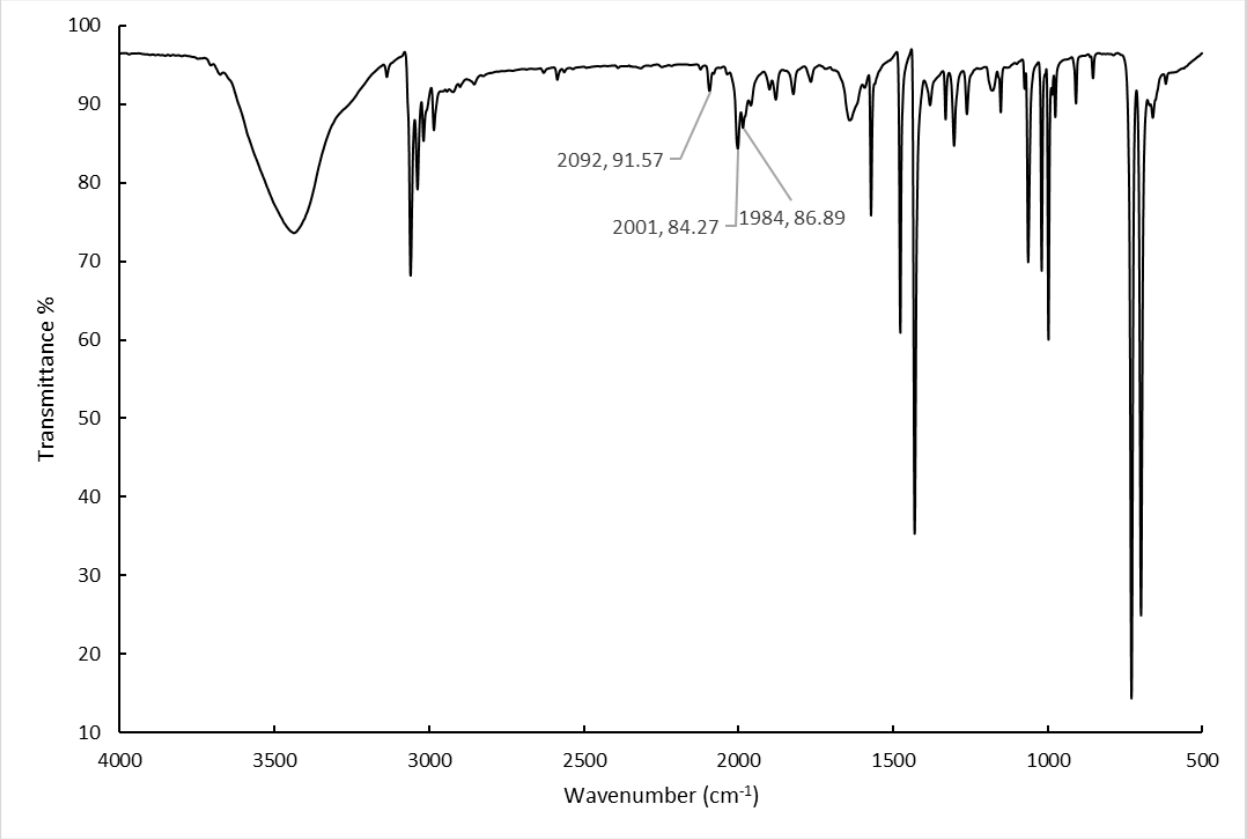

Figure 2. IR spectrum of KBr–$Mn(CO)_5PbPh_3$ pellet.

Peak Assignment	Wavenumber in cm^{-1}
CO stretch	2001
Trans C-O triple bond stretch	2092 cm^{-1}
CO stretch	1984

Table 2. IR peak assignment and wavenumbers (in cm^{-1}) of KBr–$Mn(CO)_5PbPh_3$ pellet.

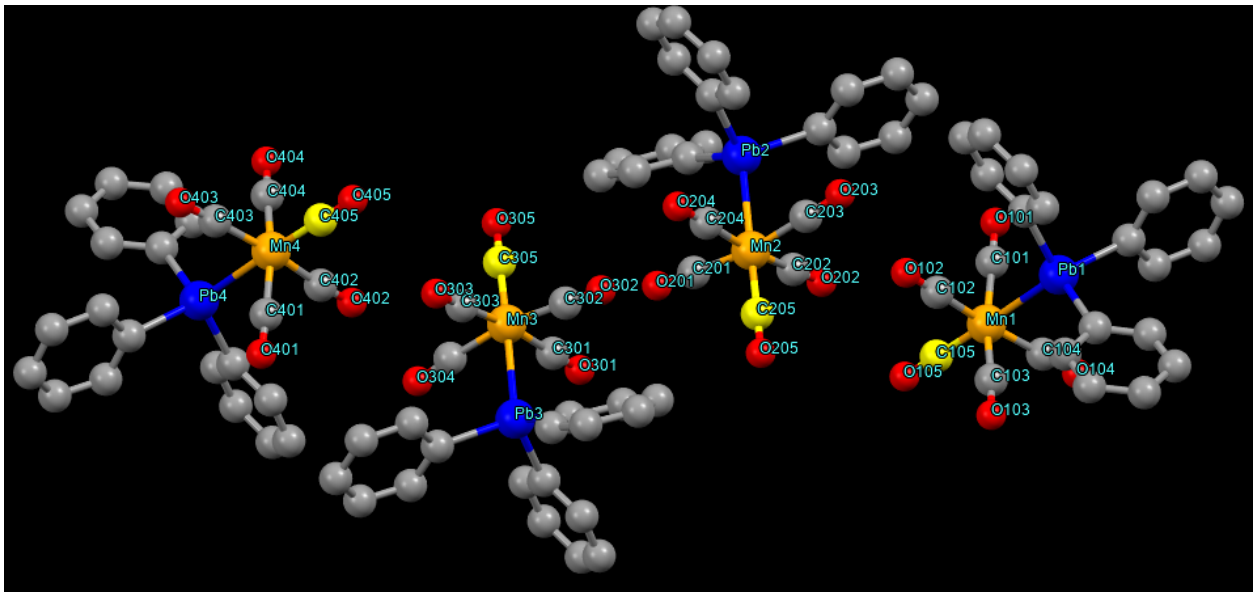

Figure 3. Structure of Single Asymmetric Unit of a crystal of $Mn(CO)_5PbPh_3$ (hydrogens have been omitted, and *trans* carbons are colored in yellow, all others in gray).

Mn Bond	*Cis* Carbon	*Cis* Length (Å) (error)	*Trans* Carbon	Length (Å)	*Cis* Carbon	*Cis* Oxygen	Length CO(Å)	*Trans* Carbon	*Trans* Oxygen	Length (Å)
Mn1	C103	1.842 (1) Å	C105	1.836 (1) Å	C402	O402	1.15 (1) Å	C405	O405	1.15 (2) Å
Mn1	C104	1.854 (1) Å	C205	1.832 (1) Å	C401	O401	1.16 (2) Å	C305	O305	1.15 (1) Å

Mn1	C102	1.846 (9) Å	C305	1.81 (1) Å	C403	O403	1.16 (1) Å	C205	O205	1.15 (1) Å
Mn1	C101	1.849 (1) Å	C405	1.816 (1) Å	C404	O404	1.14 (2) Å	C105	O105	1.14 (2) Å
Mn2	C203	1.84 (1) Å			C301	O301	1.14 (1) Å			
Mn2	C202	1.847(1) Å			C302	O302	1.14 (2) Å			
Mn2	C201	1.847 (1) Å			C303	O303	1.16 (1) Å			
Mn2	C204	1.84 (1) Å			C304	O304	1.15 (2) Å			
Mn3	C302	1.841 (1) Å			C201	O201	1.14 (2) Å			
Mn3	C301	1.848 (1) Å			C204	O204	1.13 (1) Å			
Mn3	C304	1.864 (1) Å			C203	O203	1.15 (2) Å			
Mn3	C303	1.839 (1) Å			C202	O202	1.16 (1) Å			
Mn4	C402	1.849 (9) Å			C101	O101	1.15 (2) Å			
Mn4	C401	1.856 (1) Å			C104	O104	1.14 (1) Å			
Mn4	C403	1.849 (1) Å			C103	O103	1.16 (2) Å			
Mn4	C404	1.829 (1) Å			C102	O102	1.14 (1) Å			

Table 3. $Mn(CO)_5PbPh_3$ Mn–C bonds' bond length data from Single Crystal X-Ray Crystallography.

Cis Mn–C length average length (Å)	*Cis* Mn–C length standard deviation (Å)	*Cis* Mn–C Avg - 3*Std. Dev. (Å)	*Cis* Mn–C Avg + 3*Std. Dev. (Å)	*Trans* Mn–C length average length (Å)	*Trans* Mn–C length standard deviation (Å)	*Trans* Avg - 3*Std. Dev. (Å)	*Trans* Mn–C Avg + 3*Std. Dev. (Å)
1.8459 Å	0.007971 Å	1.8220 Å	1.8698 Å	1.825 Å	0.01291 Å	1.7863 Å	1.8637 Å

Table 4. Statistical Data of $Mn(CO)_5PbPh_3$ Mn–C bonds' bond length data from Single Crystal X-Ray Crystallography.

Cis CO length average length (Å)	*Cis* CO length standard deviation (Å)	*Cis* CO Avg - 3*Std. Dev. (Å)	*Cis* CO Avg + 3*Std. Dev. (Å)	*Trans* CO length average length (Å)	*Trans* CO length standard deviation (Å)	*Trans* CO Avg - 3*Std. Dev. (Å)	*Trans* CO Avg + 3*Std. Dev. (Å)
1.1481 Å	0.00981 Å	1.1186 Å	1.177 Å	1.1475 Å	0.005 Å	1.1325 Å	1.1625 Å

Table 5. Statistical Data of $Mn(CO)_5PbPh_3$ CO bonds' bond length data from Single Crystal X-Ray Crystallography.

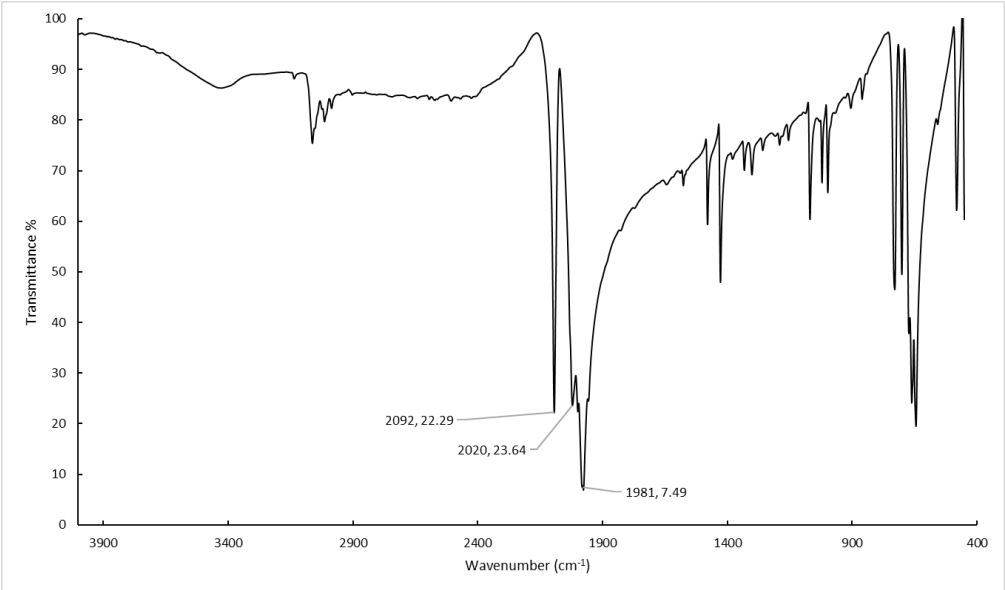

Figure 4. IR Spectrum of KBr-$Mn(CO)_5SnPh_3$ pellet.

Peak Assignment	Wavenumber in cm^{-1}
CO Stretch	2020 cm^{-1}
Trans CO Stretch	2092 cm^{-1}
CO stretch	1981 cm^{-1}

Table 6. IR peak assignments and wavenumbers (in cm^{-1}) of KBr–$Mn(CO)_5SnPh_3$ pellet.

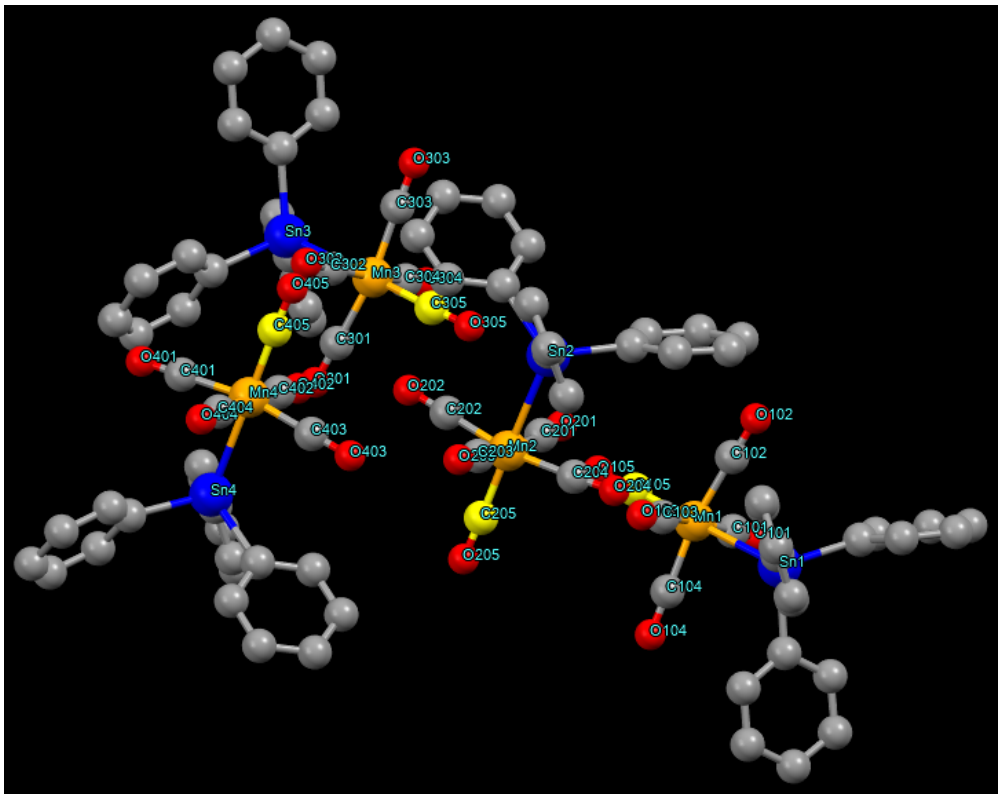

Figure 5. Structure of Single Asymmetric Unit of a crystal of $Mn(CO)_5SnPh_3$ (hydrogens have been omitted, and *trans* carbons are colored in yellow, all others in gray).

Mn Bond	*Cis* Carbon	*Cis* Length (Å) (error)	*Trans* Carbon	Length (Å)	*Cis* Carbon	*Cis* Oxygen	Length CO(Å)	*Trans* Carbon	*Trans* Oxygen	Length (Å)

Mn1	C104	1.848 (5) Å	C105	1.841 (4) Å	C101	O101	1.145 (6) Å	C105	O105	1.138 (5) Å
Mn1	C101	1.852 (5) Å	C205	1.839 (5) Å	C102	O102	1.133 (7) Å	C205	O205	1.135 (6) Å
Mn1	C103	1.848 (5) Å	C305	1.837 (4) Å	C103	O103	1.133 (6) Å	C305	O305	1.141 (5) Å
Mn1	C102	1.859 (6) Å	C405	1.83 (6) Å	C104	O104	1.141 (6) Å	C405	O405	1.146 (7) Å
Mn2	C204	1.864 (5) Å			C201	O201	1.138 Å (6)			
Mn2	C201	1.858 (5) Å			C202	O202	1.14 (5) Å			
Mn2	C203	1.843 (5) Å			C203	O203	1.143 (6) Å			
Mn2	C202	1.849 (4) Å			C204	O204	1.132 (6) Å			
Mn3	C403	1.846 (4) Å			C301	O301	1.134 (7) Å			
Mn3	C404	1.855 (5) Å			C302	O302	1.138 (6) Å			
Mn3	C401	1.869 (5) Å			C303	O303	1.145 (6) Å			
Mn3	C402	1.846 (5) Å			C304	O304	1.137 (6) Å			
Mn4	C302	1.856 (5) Å			C401	O401	1.129 (6) Å			
Mn4	C301	1.867 (6) Å			C402	O402	1.139 (6) Å			
Mn4	C303	1.844 (5) Å			C403	O403	1.134 (5) Å			
Mn4	C304	1.847			C404	O404	1.142			

		(5) Å					(6) Å			

Table 7. $Mn(CO)_5SnPh_3$ Mn–C bonds' bond length data from Single Crystal X-Ray Crystallography.

Cis Mn–C length average length (Å)	*Cis* Mn–C length standard deviation (Å)	*Cis* Mn–C Avg - 3*Std. Dev. (Å)	*Cis* Mn–C Avg + 3*Std. Dev. (Å)	*Trans* Mn–C length average length (Å)	*Trans* Mn–C length standard deviation (Å)	*Trans* Avg - 3*Std. Dev. (Å)	*Trans* Mn–C Avg + 3*Std. Dev. (Å)
1.8532 Å	0.00828 Å	1.8283 Å	1.8780 Å	1.8367 Å	0.00479 Å	1.8224 Å	1.8511 Å

Table 8. Statistical Data of $Mn(CO)_5SnPh_3$ Mn–C bonds' bond length data from Single Crystal X-Ray Crystallography.

Cis CO length average length (Å)	*Cis* CO length standard deviation (Å)	*Cis* CO Avg - 3*Std. Dev. (Å)	*Cis* CO Avg + 3*Std. Dev. (Å)	*Trans* CO length average length (Å)	*Trans* CO length standard deviation (Å)	*Trans* CO Avg - 3*Std. Dev. (Å)	*Trans* CO Avg + 3*Std. Dev. (Å)
1.1.1377 Å	0.00484 Å	1.1232 Å	1.1522 Å	1.1400 Å	0.00469 Å	1.1259 Å	1.1541 Å

Table 9. Statistical Data of $Mn(CO)_5SnPh_3$ CO bonds' bond length data from Single Crystal X-Ray Crystallography.

DISCUSSION

The electronic structure of the octahedral, 6 d-electron metal center compounds, $Mn(CO)_5EPh_3$ (where E = Pb or Sn), which includes the d-orbital splitting, is shown below in figure 6. Moreover, since the target compounds both consist of a *strong* ligand field strength due to the presence of 5 carbonyls,

they are expected to be low-spin complexes. Moreover, the data that supports this assertion is the NMR spectra itself – which could only be produced if the species at hand were diamagnetic and low-spin. Moreover, the two empty CO π^* molecular orbitals interact with the D_{XY}, D_{XZ}, and D_{YZ} d-orbitals and act as π-acceptors, and the lone pair on C in CO acts as a σ-donor to form a single bond with the $D_{x^2-y^2}$ or the D_{Z^2} orbital from the Mn(I) atoms.

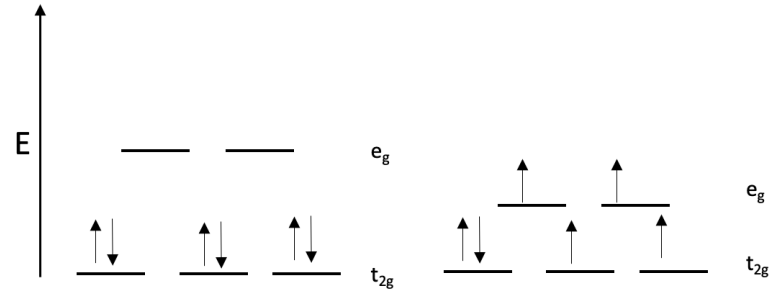

Figure 6. D-orbital splitting of $Mn(CO)_5EPh_3$ (where E = Pb, Sn) with low-spin (left, correct spin) and high-spin (right, incorrect spin) orientations.

The molecular structures of the starting materials for $Mn(CO)_5EPh_3$ are depicted in figure 7 below. In addition, the molecular structures of the products, $Mn(CO)_5EPh_3$ and Ph_3PbCl, are depicted in figure 8.

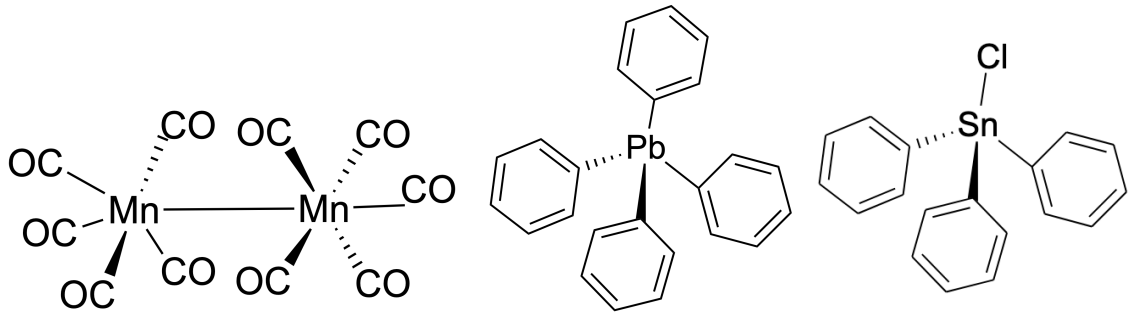

Figure 7. Molecular structures of the starting materials $Mn_2(CO)_{10}$, Ph_4Pb, and Ph_3SnCl.

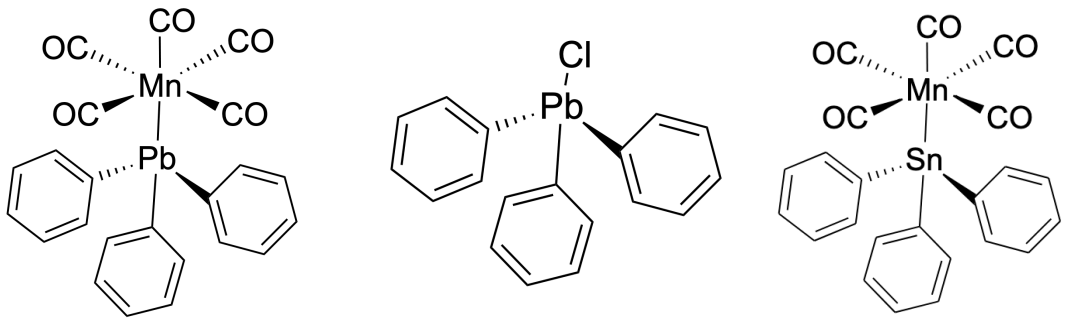

Figure 8. Molecular structures of $Mn(CO)_5EPh_3$, where E = Pb or Sn, and Ph_3PbCl.

The mechanism for the synthesis of Ph_3PbCl, which is tetrahedral in structure, is discussed as follows: the generation of HCl is required in order for the phenyl ring in the starting material Ph_4Pb to act as a leaving group, so NaCl and H_2SO_4 react to form HCl, from which then, in a concerted mechanism, Cl^- can attack the Pb center in Ph_4Pb while simultaneously, a phenyl ring from Ph_4Pb grabs the proton from HCl to give the product Ph_3PbCl and the byproduct benzene. Equations (1) and (2) are shown below to depict the balanced reactions for this synthesis of Ph_3PbCl.

$$2NaCl + H_2SO_4 \rightleftharpoons 2HCl + Na_2SO_4 \quad (1)$$

$$HCl + Ph_4Pb \longrightarrow Ph_3PbCl + \text{benzene} \quad (2)$$

Ph_3ECl (where E = Pb, Sn) was used in the synthesis of the target compound $Mn(CO)_5EPh_3$ (E= Pb, Sn): the two manganese(0) metal centers in $Mn_2(CO)_{10}$ react with Na(0) (reductant) in the presence of mercury and get reduced to produce two nucleophilic pentacarbonylmanganese(-1) compounds, each of which acts as a nucleophile to attack the Ph_3ECl with chlorine then acting as a leaving group to produce the product $Mn(CO)_5EPh_3$ and the byproduct sodium chloride. Equation 3 below is shown to depict the balanced reaction for this synthesis.

$$Mn_2(CO)_{10} + 2Na(0) + Hg(0) + 2Ph_3ECl \longrightarrow 2\ Mn(CO)_5EPh_3 + 2NaCl + Hg(0) \quad (3)$$

Characterization of Ph_3PbCl and $Mn(CO)_5EPh_3$ (where E = Pb, Sn) using NMR and IR spectroscopy, and X-Ray crystallography was used to answer the question whether -$PbPh_3$ or -$SnPh_3$ have a greater or

lesser *trans* influence than one another. Asserting the relative bond strengths of the *trans* Mn–C bonds could theoretically provide insight into this question, and the following discussion has been used to predict whether a *trans* influence existed or not by studying the IR and X-Ray crystallography data, with the exception to NMR spectroscopy, which was only used to assess whether the correct molecules were present in samples.

Theoretical predictions for the ^{1}H NMR for all three spectra are expected to be the same, with the only difference being in the amount of deshielding that occurs when ^{207}Pb and ^{119}Sn atoms are considered. It can be concluded that three different proton NMR signals would be expected, as the H-ortho protons, the H-meta protons, and the H-para protons are all chemically inequivalent (see figure 9). From this point on, due to the presence of the E atom in the ligand (where E = Pb or Sn), it can be concluded that the H-ortho protons' nuclei would be most deshielded and the H-para proton's nucleus would be least deshielded; therefore, the order of the three signals is: H-ortho signal (highest ppm) → H-meta signal → H-para signal (lowest ppm). Moreover, it can be expected that due presence of 2 H-ortho protons, 2 H-meta protons, and 1 H-para proton, the integration ratio between the three signals would be 1 to 1 to 0.5, or 2:2:1.

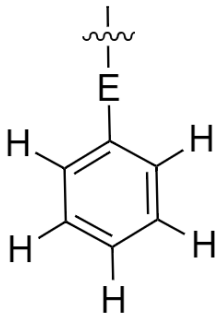

Figure 9. Molecular structure of -EPh$_3$ ligand (where E = Pb, or Sn) showing the ^{1}H protons involved in ^{1}H NMR splitting.

The theoretical NMR splitting prediction of the H-ortho protons is considered first. It is known that the ^{207}Pb atom is abundant in nature approximately 22% of the time[12], and the ^{1}H protons are

present approximately 99% of the time; therefore, about 22% of the time, the H-ortho protons would couple to the 3 bond lengths away ^{207}Pb atom, which would result a superposition of the Pb and H-meta and H-para splittings, which is depicted below in figure 10.

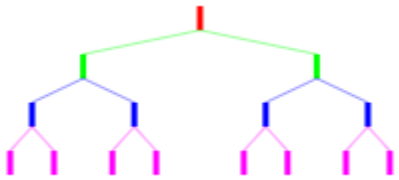

Figure 10. Branching tree diagram of the H-ortho splitting that occurs 22% of the time due to the ortho proton coupling with the ^{207}Pb atom ($^{3}J_{H\text{-}Pb}$ in green, $^{3}J_{H\text{-}H}$ in blue, $^{4}J_{H\text{-}H}$ in pink).[11]

About 22% of the time, H-ortho would couple to the 3 bond lengths away H-meta proton as a doublet, to the 3 bond lengths away ^{207}Pb atom as a doublet, and to the 4 bond lengths away H-para proton as a doublet as well, resulting in a doublet of doublet of doublets. This H-ortho superposition splitting pattern prediction is supported by the NMR data for all three compounds (see appendix), where the $^{3}J_{H\text{-}Pb}$ was seen as a doublet, and the $^{3}J_{H\text{-}H}$ was seen as a doublet, but the $^{4}J_{H\text{-}H}$ doublet was not resolved.

Additionally, 78% of the time, the H-ortho would split into a doublet by the $^{3}J_{H\text{-}H}$ H-meta and the $^{4}J_{H\text{-}H}$ H-para proton as a doublet, resulting in a doublet of doublets. However, in our NMR spectra, only a doublet arising from the $^{3}J_{H\text{-}H}$ is resolved enough to see, and the second $^{4}J_{H\text{-}H}$ H-para proton doublet cannot be seen.

The H-meta splitting prediction is discussed as follows. The H-meta proton would be split by the $^{3}J_{H\text{-}H}$ H-para and H-ortho protons as a triplet, and the $^{4}J_{H\text{-}E}$ E atom as a doublet. This prediction is supported by NMR data for Ph_3PbCl (see appendix), but not for $Mn(CO)_5PbPh_3$, where only the triplet from $^{3}J_{H\text{-}H}$ can be noticed, and also not for $Mn(CO)_5SnPh_3$, where the H-ortho, H-para, and the $^{3}J_{H\text{-}Sn}$ is seen as a multiplet.

The H-para splitting prediction is discussed as follows. The H-para proton would be split by the $^{3}J_{H\text{-}H}$ H-meta protons as a triplet, by the $^{4}J_{H\text{-}H}$ H-ortho protons as a triplet, and by the $^{5}J_{H\text{-}E}$ E atom as a doublet (22% of the time). The overall splitting would be a triplet of triplet of doublets. And the other 78% of the time, as a triplet of triplets. This prediction is partially supported by the Ph_3PbCl and $Mn(CO)_5PbPh_3$ NMR Spectra (see appendix) where the $^{3}J_{H\text{-}H}$ H-meta splitting can be noticed as a triplet, but the $^{4}J_{H\text{-}H}$ from H-ortho nor the $^{5}J_{H\text{-}E}$ from the E atoms can be noticed for all compounds. For $Mn(CO)_5SnPh_3$, neither the $^{3}J_{H\text{-}H}$ nor the $^{3}J_{H\text{-}H}$ nor the $^{3}J_{H\text{-}H}$ can be resolved - therefore, the H-para splitting for this compound is resolved only as a multiplet.

It is important to be noted that 22% of the time, both the H-meta and H-para protons would split as a superposition of the E-atoms and the other H protons; however, the respective branching diagrams have been not been discussed since it was done once already for H-ortho proton.

Moreover, it should be noted that ^{119}Sn has a relative abundance of 8.6%[13], so this percent of the time, the H-protons are expected to be split by the Sn atom.

The *trans* influence of ligands is essentially described as a thermodynamic phenomenon in which a ligand can weaken the bond strength of the metal-ligand' bond *trans* to it. The influence of $-PbPh_3$ vs $-SnPh_3$ was studied using IR and X-Ray data. Both complexes are expected to have the same point group of C_{4v}, and if all ligands are considered as spheres, the reducible representation as a result of applying E, $2C_4$, C_2, $2\sigma_V$, and $2\sigma_D$ to these spheres is: $\Gamma = 5\ 1\ 1\ 3\ 1$, and the decomposition of this reducible representation into an irreducible representation gives (since h = 8) is $\Gamma = 2A_1 + B_1 + E$, where $2A_1$ and E are expected to be the IR active vibrational modes. In total, 3 carbonyl peaks are to be expected: one from the *trans* A_1 CO vibration, one from another A_1 vibration, and 1 from the E vibrational mode. Moreover, the *trans* CO peak from the A_1 vibrational mode is expected to have the highest frequency. From the IR data, the *trans* CO peak for $Mn(CO)_5PbPh_3$ and for $Mn(CO)_5SnPh_3$ are shown to both have a CO stretching frequency of 2092 cm^{-1}.

Since both of the -EPh_3 have the same *trans* CO stretching frequencies, it can be inferred that the *trans* Mn–C bond strengths of both complexes are of equal magnitude, implying that -$PbPh_3$'s trans influence is no greater or lesser than -$SnPh_3$'s *trans* influence.

In addition to the IR data, X-ray crystallography data is also expected to provide insight into the question as to whether a trend in the *trans* influence exists for -EPh_3 ligands (where E = a group 14 element). In a single asymmetric unit of both of the crystals, 4 copies of $Mn(CO)_5EPh_3$ were present, and therefore, in order to study the *trans* influence, averages across all *trans* Mn–C, *trans* CO, and *cis* Mn–C, and *cis* CO bonds were taken, and a statistically significant range of -3*standard deviation for each type of bond was made (see tables 4, 5, 8, and 9). The *trans* Mn–C bonds were compared to the *cis* Mn–C bonds in $Mn(CO)_5PbPh_3$, and it was found that the *trans* Mn–C bonds were not statistically significantly shorter than the *cis* Mn–C bonds (see table 4). This directly showed that the *trans* influence of -$PbPh_3$ relative to any *cis*-carbonyl within $Mn(CO)_5PbPh_3$ was not greater or lesser. The same was found to be true for the *trans* Mn–C bonds with the *cis*-Mn–C bonds for $Mn(CO)_5SnPh_3$ (see table 8). In addition, the *trans* CO bonds within $Mn(CO)_5PbPh_3$ and within $Mn(CO)_5SnPh_3$ were not statistically significantly shorter than the *cis*-CO bonds within those same compounds (see table 5 and 9), suggesting that the relative bond strengths of the *trans* Mn–C bonds within each molecule were not statistically significantly different from the *cis* Mn–C bond strengths.

However, these assertions don't indicate any insight into the research question. It is the comparison of the *trans* Mn–C bonds within $Mn(CO)_5PbPh_3$ to the *trans* Mn–C bonds of $Mn(CO)_5SnPh_3$ that is expected to provide insight into the *trans* influence of -$PbPh_3$ versus -$SnPh_3$. Therefore, according to tables 4 and 8, it can be concluded that the statistical significance ranges for *trans* Mn–C bonds across the both compounds have great overlap between each other, suggesting that -$PbPh_3$'s *trans* influence is not greater or lesser than the *trans* influence of -$SnPh_3$. And the two compounds' *trans* CO bonds are also not statistically significantly different. If they were, insight would be provided into the bond strength

differences in the *trans* Mn–C bonds, and therefore into the *trans* influence of -$PbPh_3$ and -$SnPh_3$, but it is clear that no such difference in the *trans* influence exists.

CONCLUSION

Based on the findings in this report, it can be concluded that a statistically significant difference in the *trans* influence between -$PbPh_3$ and -$SnPh_3$ ligands in $Mn(CO)_5PbPh_3$ and $Mn(CO)_5SnPh_3$ does not exist. This conclusion is supported firstly by the IR data and secondly by the X-Ray crystallography data. The IR data showed that the *trans* CO vibrational frequency of $Mn(CO)_5PbPh_3$ and $Mn(CO)_5SnPh_3$ were exactly the same. The vibrational frequency of a bond is directly proportional to the force constant of that bond – therefore, the stronger the CO vibrational frequency the stronger the *trans* CO bond, and therefore, the weaker the *trans* Mn–C bond. However, if both of the *trans* CO vibrational frequencies are identical, then naturally the bond strengths of the *trans* Mn–C bonds in $Mn(CO)_5PbPh_3$ and $Mn(CO)_5SnPh_3$ are equally as strong, and therefore, there is no difference in the *trans* influence of -$PbPh_3$ versus -$SnPh_3$ ligands. To further support this finding, the crystallographic data was considered, and it was found that there exists no statistically significant difference between the *trans* Mn–C bond lengths of $Mn(CO)_5PbPh_3$ and $Mn(CO)_5SnPh_3$; therefore, it is a natural conclusion that there exists no statistically significant difference in the *trans* influence of -$PbPh_3$ and -$SnPh_3$ ligands.

REFERENCES

1. Tsipis, A. C., Trans-Philicity (Trans-Influence/Trans-Effect) Ladders for Square Planar Platinum(II) Complexes Constructed by 35Cl NMR Probe. *J. Comp. Chem.* **2019**, *40* (29), 2550–2562.

2. Baik, M.H.; Friesner, R. A.; Lippard, S. J. Theoretical Study of Cisplatin Binding to Purine Bases: Why Does Cisplatin Prefer Guanine over Adenine? *J. Am. Chem. Soc.* **2003**, *125* (46), 14082–14092.
3. Pinter, B.; Van Speybroeck, V.; Waroquier, M.; Geerlings, P.; De Proft, F. Trans Effect and Trans Influence: Importance of Metal Mediated Ligand-Ligand Repulsion. Phys. Chem. Chem. Phys. **2013**, *15* (40), 17354–17365.
4. He, J.; Jiang, H.; Takise, R.; Zhu, R.-Y.; Chen, G.; Dai, H.-X.; Dhar, T. G.; Shi, J.; Zhang, H.; Cheng, P. T.; Yu, J.-Q. Ligand-Promoted Borylation of C(sp^3)-H Bonds with Palladium(Ii) Catalysts. *Angewandte Chemie International Edition* **2015**, *55* (2), 785–789.
5. Gholivand, K.; Mahzouni, H. R. Trans Influence and Covalent Bonding in a New Octahedral Lanthanum(Iii) Complex of Diphenylmorpholinyl Phosphinamide. *Inorganica Chimica Acta* **2012**, *386*, 8–12.
6. Krogh-Jespersen, K.; Romanelli, M. D.; Melman, J. H.; Emge, T. J.; Brennan, J. G. Covalent Bonding and the Trans Influence in Lanthanide Compounds. *J. Inorg. Chem.* **2009**, 49 (2), 552–560.
7. Moreno-Alcántar, G.; Hernández-Toledo, H.; Guevara-Vela, J. M.; Rocha-Rinza, T.; Martín Pendás, Á.; Flores-Álamo, M.; Torrens, H. Stability and *Trans* Influence in Fluorinated Gold(I) Coordination Compounds. *European Journal of Inorganic Chemistry* **2018**, *2018* (40), 4413–4420.
8. Katsu, T.; Hashimoto, T. Triphenyllead Chloride as a New Ionophore for an Iodide-Selective Membrane Electrode. *Analytical Letters* **1999**, *32* (4), 665–675.
9. Medvedev, A. G.; Grishanov, D. A.; Mikhaylov, A. A.; Churakov, A. V.; Tripol'skaya, T. A.; Ottenbacher, R. V.; Bryliakov, K. P.; Shames, A. I.; Lev, O.; Prikhodchenko, P. V. Triphenyllead Hydroperoxide: A 1D Coordination Peroxo Polymer, Single-Crystal-to-Single-Crystal Disproportionation to a Superoxo/Hydroxo Complex, and Application in Catalysis. *Inorganic Chemistry* **2022**, *61* (21), 8193–8205.

10. Hübner, D.; Kaluđerović, M. R.; Gómez-Ruiz, S.; Kaluđerović, G. N. Anionic Chlorido(Triphenyl)Tin(Iv) Bearing*n*-Phthaloylglycinato or 1,2,4-Benzenetricarboxylato 1,2-Anhydride Ligands: Potential Cytotoxic and Apoptosis-Inducing Agents against Several Types of Cancer. *Chemical Biology & Drug Design* **2016**, *89* (4), 628–633.
11. http://www.cheminfo.org/Spectra/NMR/Tools/Multiplet_simulator/index.html (accessed 2023-06-09).
12. https://physics.nist.gov/cgi-bin/Compositions/stand_alone.pl?ele=Pb (accessed 2023-06-09).
13. https://physics.nist.gov/cgi-bin/Compositions/stand_alone.pl?ele=Sn (accessed 2023-06-09).

APPENDIX

1. **NMR SPECTRA:**

   a. **Full ^{1}H NMR of Ph_3PbCl**

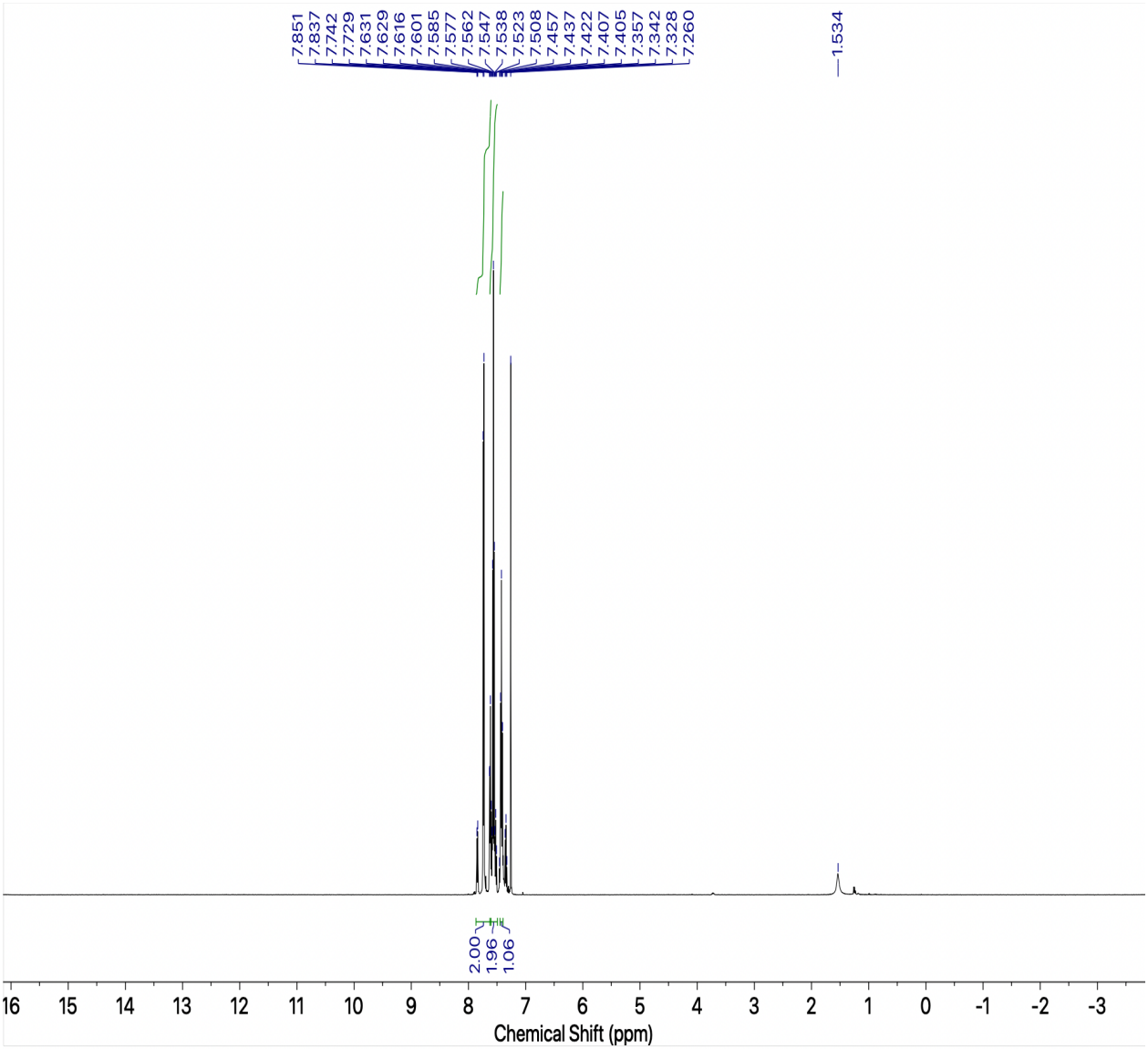

   b. **Zoomed ^{1}H NMR of Ph_3PbCl**

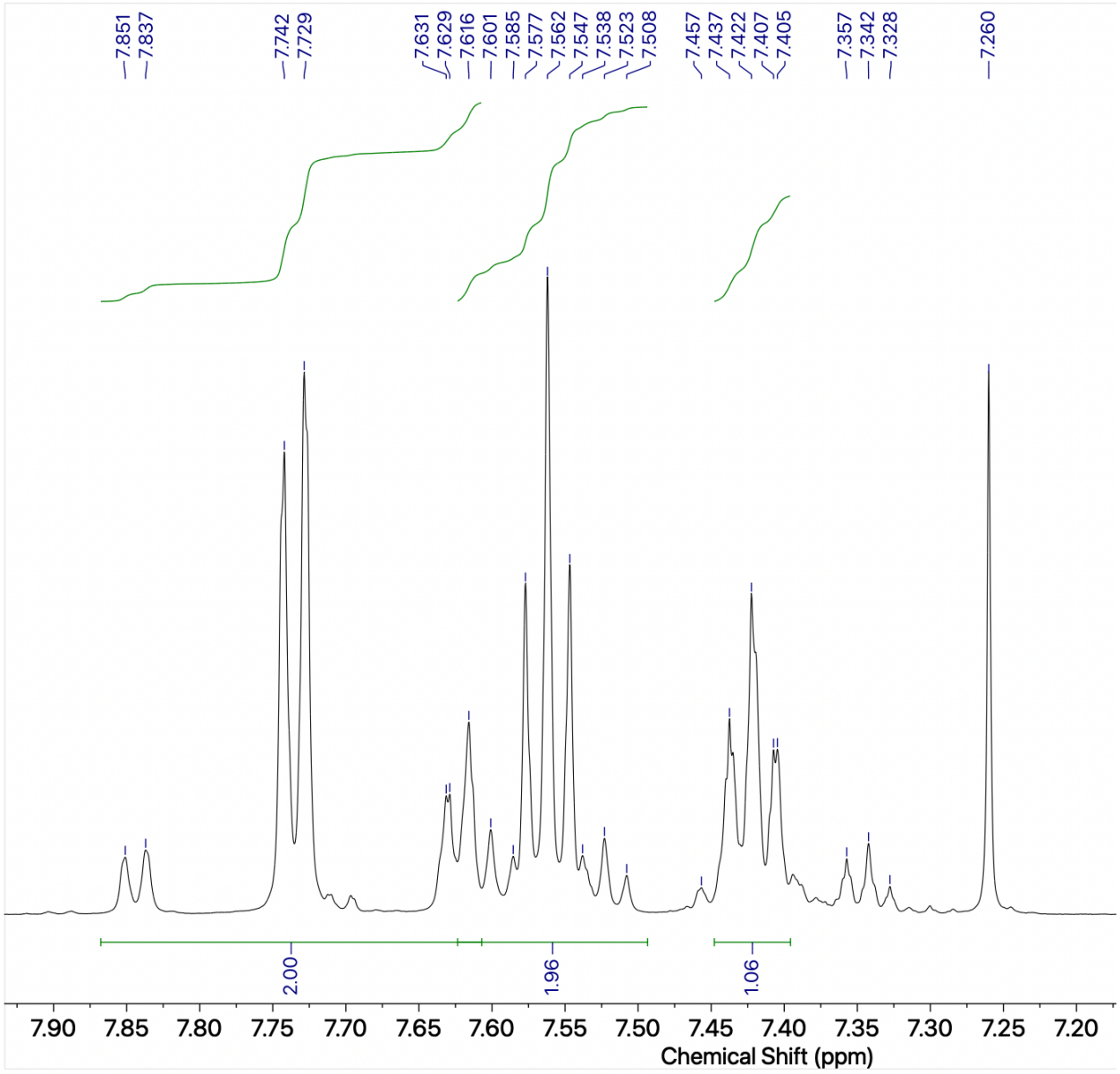

c. Full ^{207}Pb NMR spectra of Ph_3PbCl:

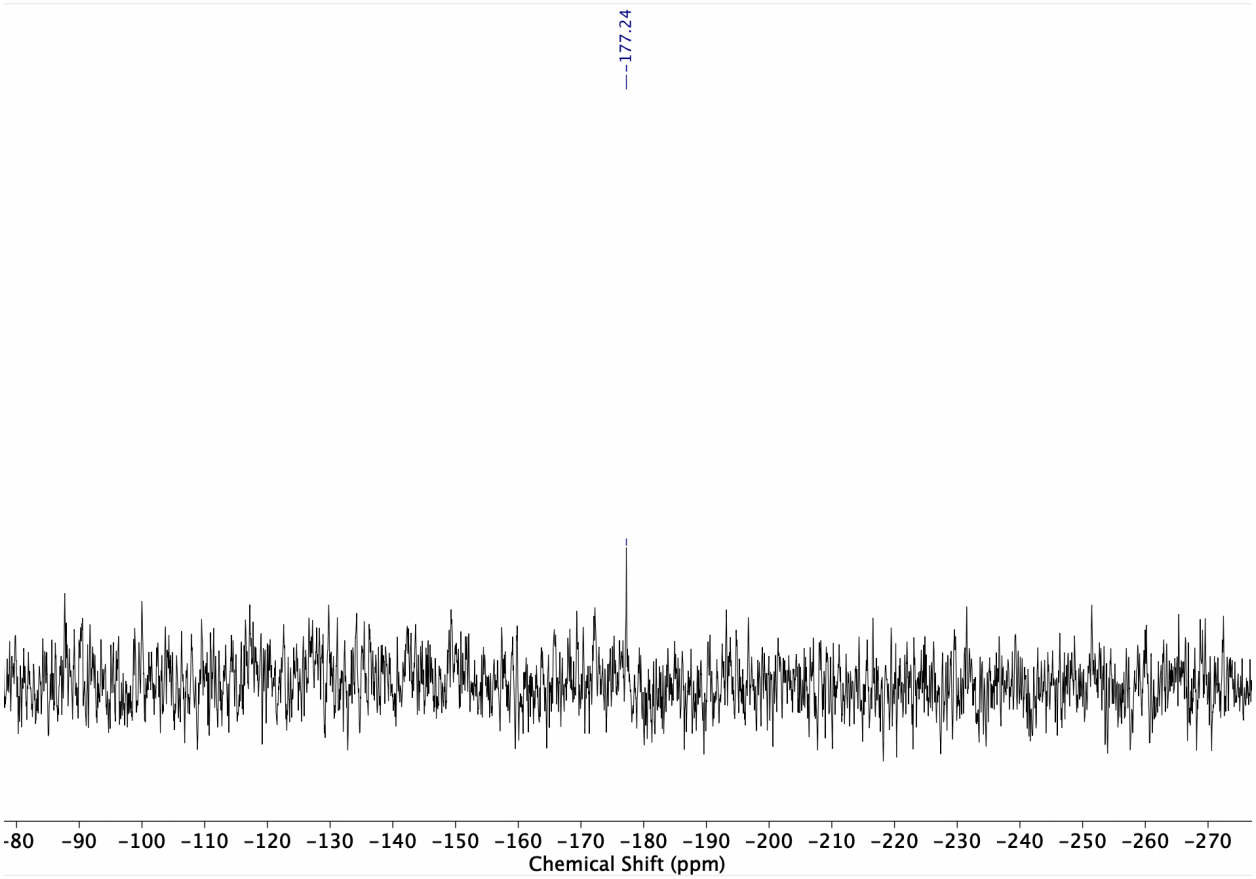

2. NMR Spectra of $Mn(CO)_5PbPh_3$:

a. Full ^{207}Pb NMR spectra of $Mn(CO)_5PbPh_3$:

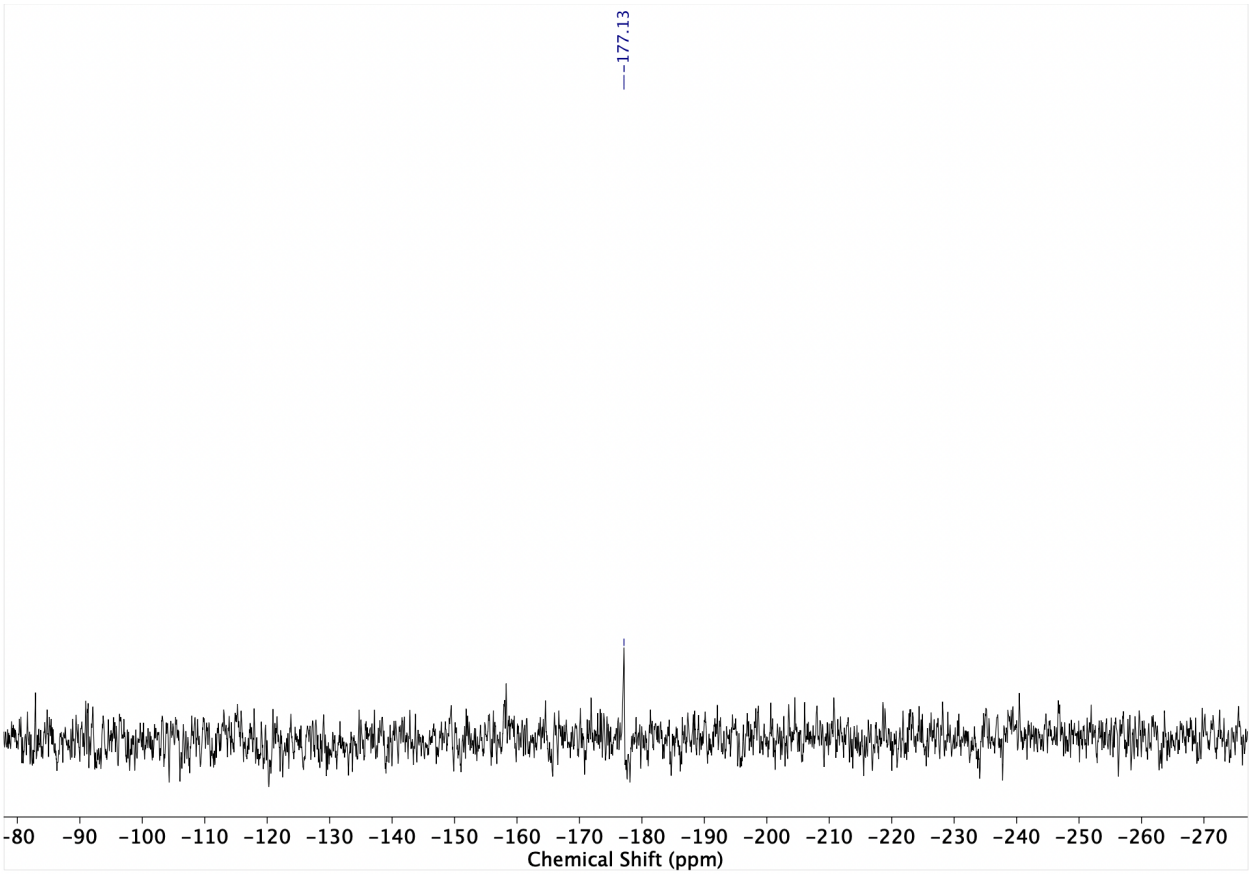

b. Full ^{1}H NMR spectra of $Mn(CO)_5PbPh_3$:

c.

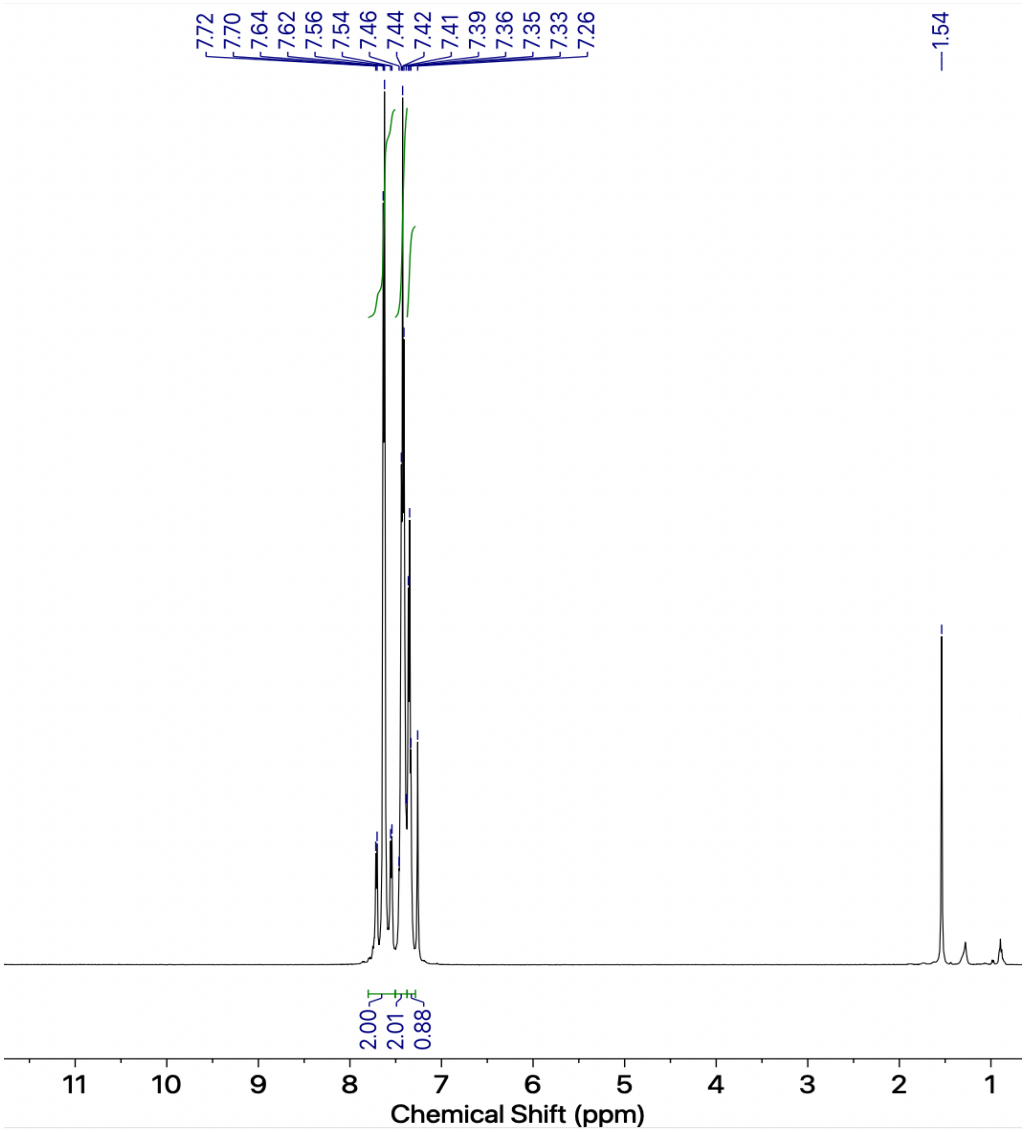

d. Zoomed ^{1}H NMR spectra of $Mn(CO)_5PbPh_3$:

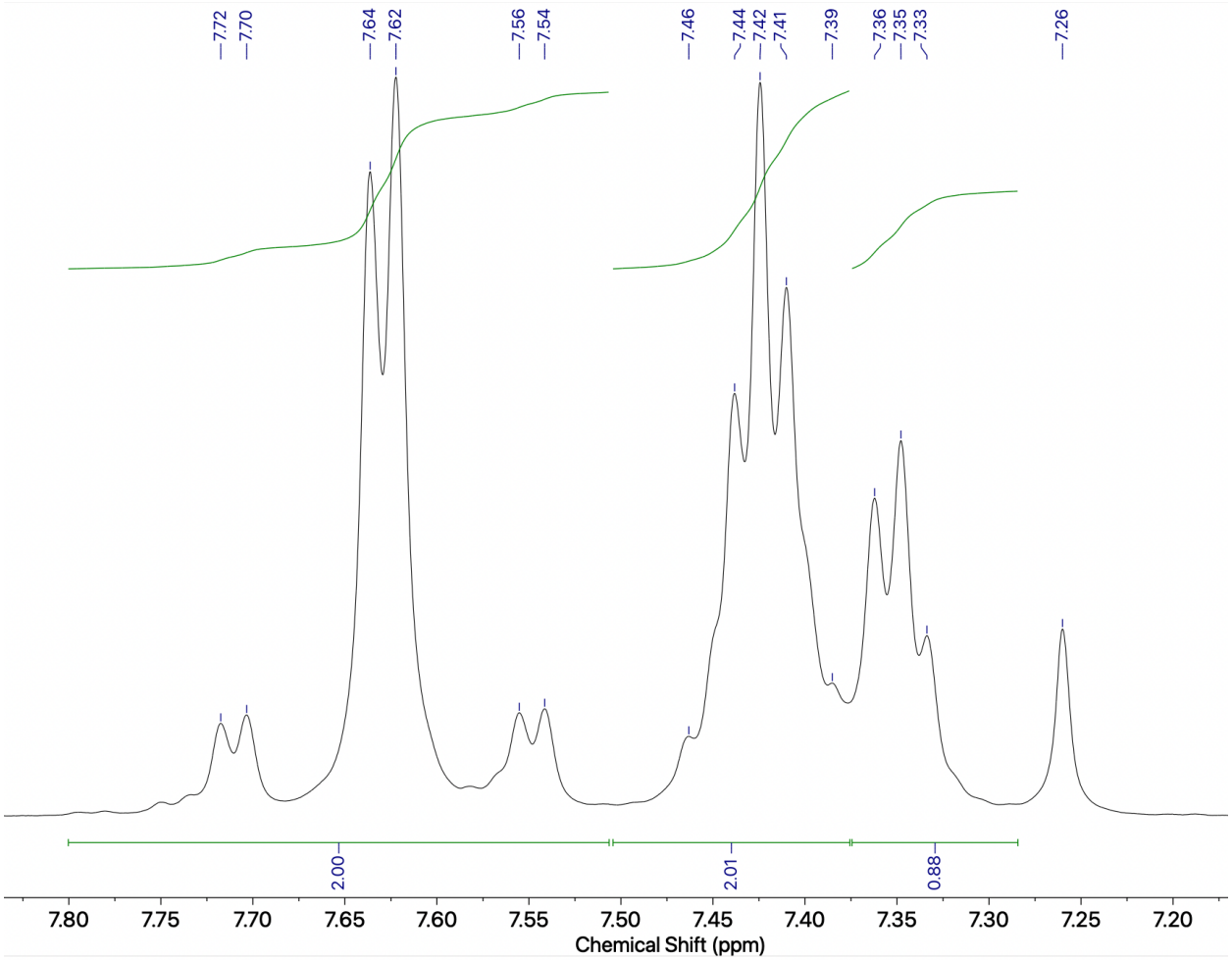

3. NMR Spectra of $Mn(CO)_5SnPh_3$:

a. Full ^1H NMR spectra of $Mn(CO)_5SnPh_3$:

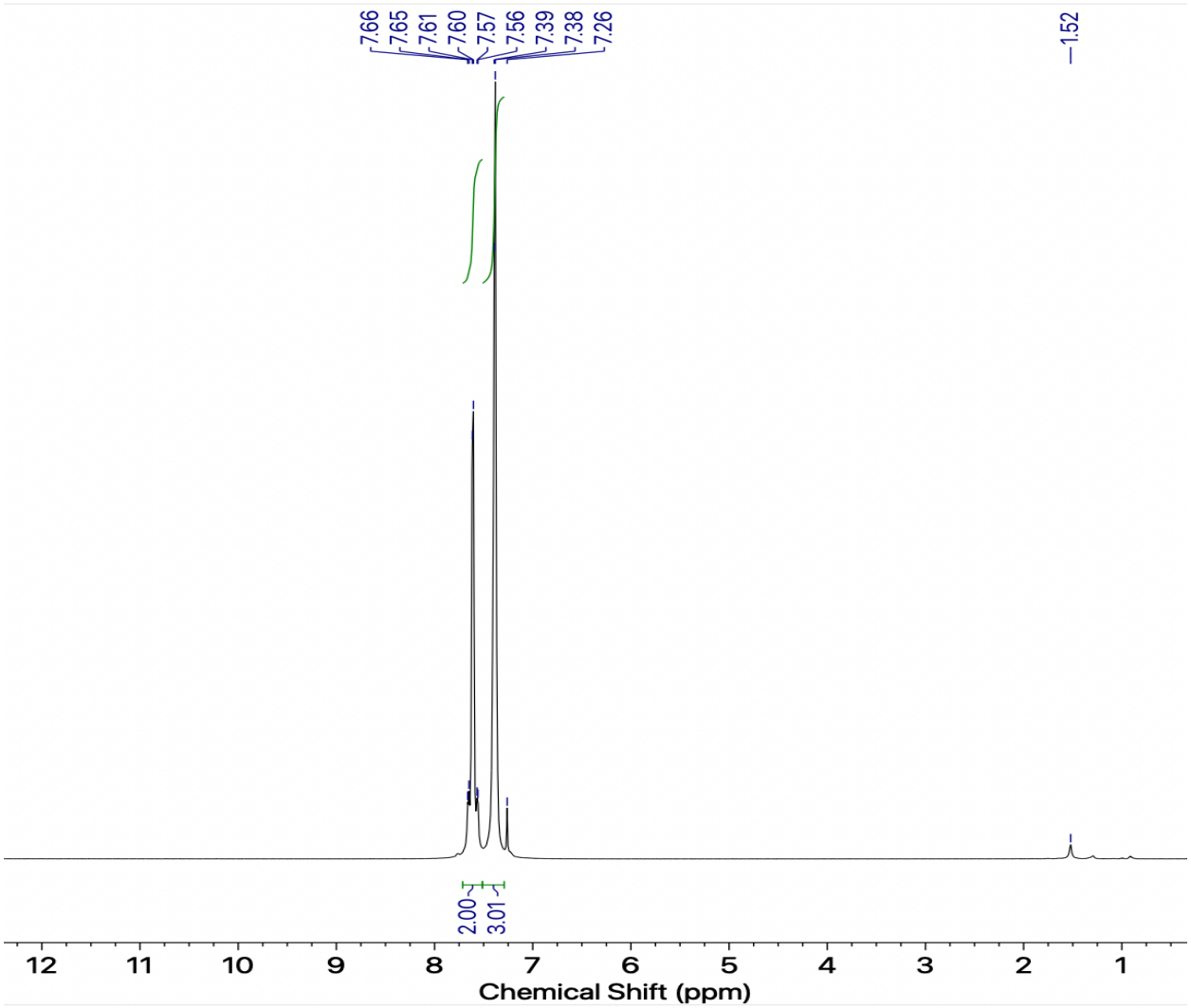

b. Zoomed ^{1}H NMR spectra of $Mn(CO)_5SnPh_3$:

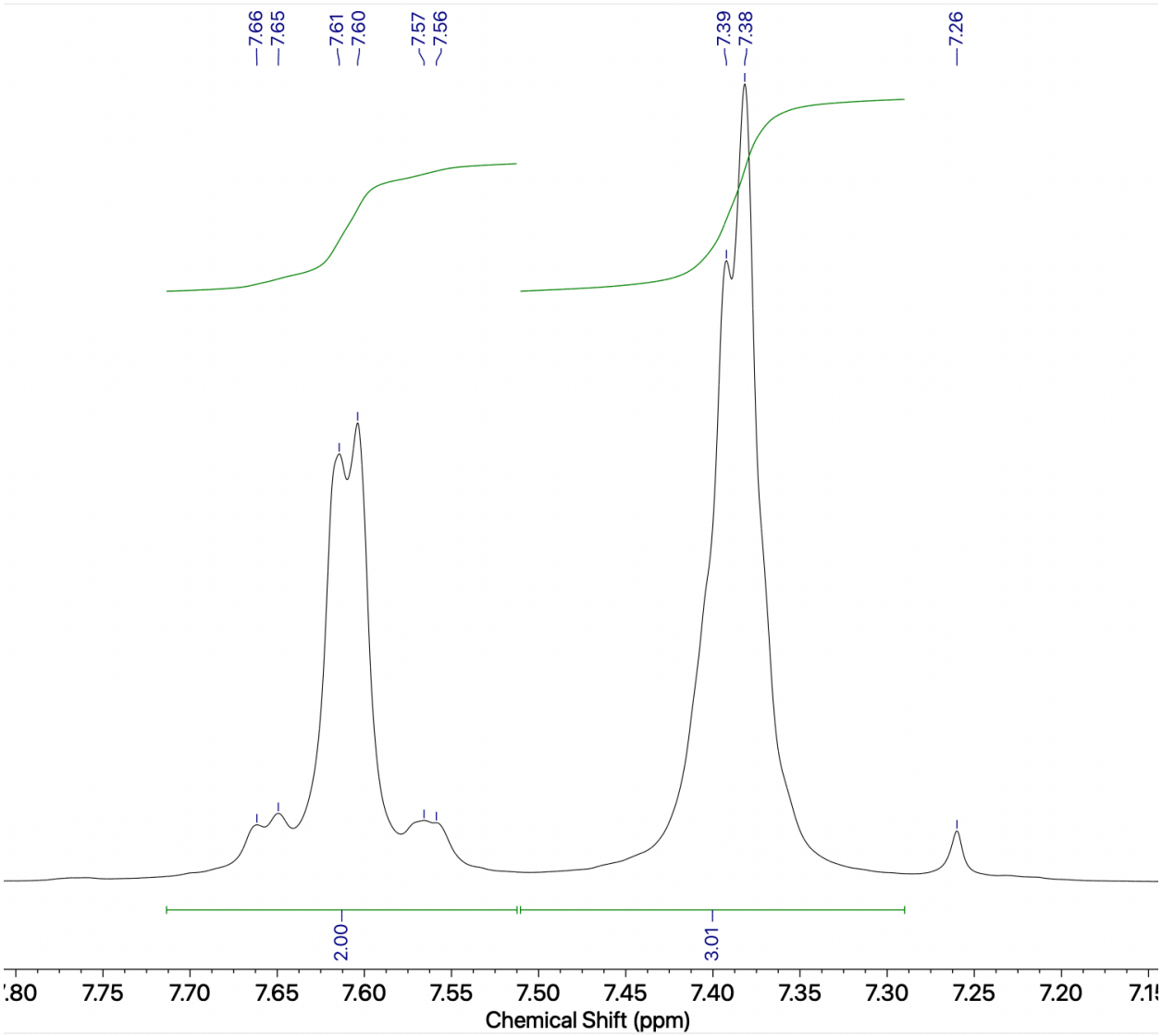

c. Full ^{119}Sn NMR spectra of $Mn(CO)_5SnPh_3$:

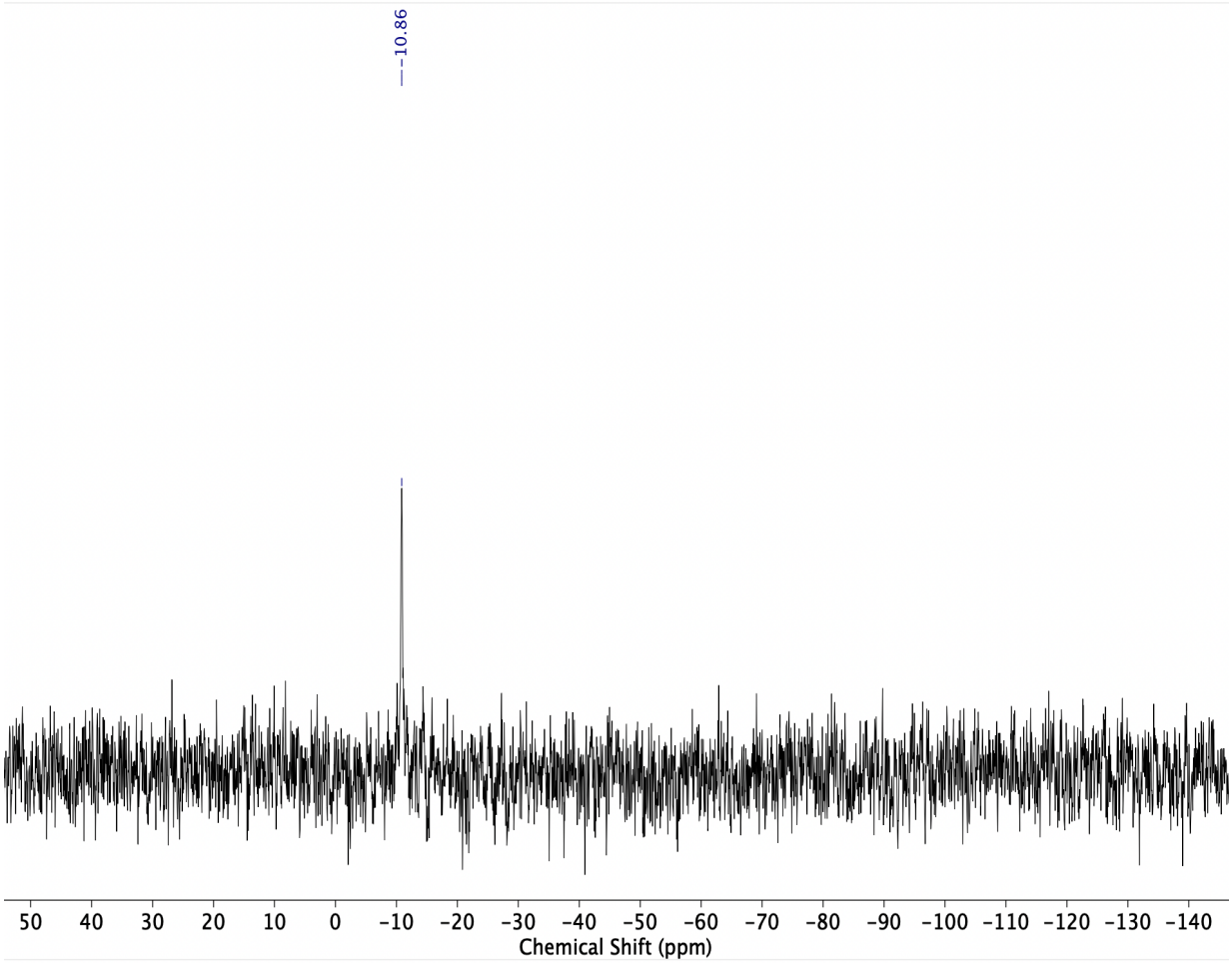
10.86
50 40 30 20 10 0 -10 -20 -30 -40 -50 -60 -70 -80 -90 -100 -110 -120 -130 -140
Chemical Shift (ppm)